catalysts

MDPI

Article

Preparation and Performance of Modified Red Mud-Based Catalysts for Selective Catalytic Reduction of NO_x with NH_3

Jingkun Wu, Zhiqiang Gong, Chunmei Lu *, Shengli Niu, Kai Ding, Liting Xu and Kang Zhang

Department of Energy and Power Engineering, Shandong University, Jinan 250061, China; jkwu@mail.sdu.edu.cn (J.W.); gongzq@gmail.com (Z.G.); nsl@sdu.edu.cn (S.N.); 18818223769@163.com (K.D.); 15165315337@163.com (L.X.); sdnengdongzk@163.com (K.Z.)

* Correspondence: cml@sdu.edu.cn; Tel.: +86-151-6686-2166

Received: 16 December 2017; Accepted: 17 January 2018; Published: 19 January 2018

Abstract: Bayer red mud was selected, and the NH_3-SCR activity was tested in a fixed bed in which the typical flue gas atmosphere was simulated. Combined with XRF, XRD, BET, SEM, TG and NH_3-Temperature Programmed Desorption (TPD) characterization, the denitration characteristics of Ce-doped red mud catalysts were studied on the basis of alkali-removed red mud. The results showed that typical red mud was a feasible material for denitration catalyst. Acid washing and calcining comprised the best treatment process for raw red mud, which reduced the content of alkaline substances, cleared the catalyst pore and optimized the particle morphology with dispersion. In the temperature range of 300–400 °C, the denitrification efficiency of calcined acid washing of red mud catalyst (ARM) was more than 70%. The doping of Ce significantly enhanced NH_3 adsorption from weak, medium and strong acid sites, reduced the crystallinity of α-Fe_2O_3 in ARM, optimized the specific surface area and broadened the active temperature window, which increased the NO_x conversion rate by an average of nearly 20% points from 250–350 °C. The denitration efficiency of $Ce_{0.3}$/ARM at 300 °C was as high as 88%. The optimum conditions for the denitration reaction of the $Ce_{0.3}$/ARM catalyst were controlled as follows: Gas Hourly Space Velocity (GHSV) of 30,000 h^{-1}, O_2 volume fraction of 3.5–4% and the NH_3/NO molar ratio ([NH_3/NO]) of 1.0. The presence of SO_2 in the feed had an irreversible negative effect on the activity of the $Ce_{0.3}$/ARM catalyst.

Keywords: red mud; deNO_x catalyst; NH_3-SCR; acid washing and calcining; cerium

1. Introduction

Red mud, which is a major solid waste derived from the aluminum industry, has been producing in huge quantities over the decades. At present, most of the red mud is treated for landfilling, which brings a heavy burden to the environment. At the same time, Bayer red mud is considered hazardous due to its strong alkalinity (pH = 10–12). Therefore, utilization of red mud has become the focus of study and an urgent issue all over the world. Since red mud contains Fe_2O_3 (20–50%) and large amounts of stable materials (SiO_2, Al_2O_3 and TiO_2), it is a potential alternative catalyst in wastewater and exhaust cleaning [1–5], which provides a cost-effective route of controlling waste by waste. However, the large-scale catalysis application of red mud is limited because of its alkalinity [6], mainly originating from Na and Ca, and their oxides can cause sintering in the catalyst and reduce the catalytic activity [7]. Recently, Li et al. [8] developed a ball milling and acid-base neutralization method to reuse red mud as an efficient Fe-Ti/Si-Al denitration catalyst free of alkali. Cao et al. [9] reported an approach that used hydrochloric acid to treat red mud followed by alkali precipitation, by which the alkaline reduced and the CO catalytic oxidation performance was improved. Besides, for the first time, Lamonier et al. [10] compared the denitration performance of raw red mud and Cu-doped

red mud, improving the activity of red mud. After that, Rajanikanth et al. [11,12] used red mud as a NO_x adsorbent, which was arranged after the plasma purifier in the tail gas treatment module of a biodiesel engine, and the results showed that in this system, most exhausted NO_2 can be converted. Nevertheless, few studies have involved red mud deNO_x catalyst in coal-fired flue gas processing.

Selective Catalytic Reduction of NO_x with NH_3 (NH_3-SCR) is the most efficient method that has been applied in many thermal power plants for flue gas denitrification, while its technical core is the SCR catalyst with high efficiency and stability. So far, the commercial SCR deNO_x catalyst is V_2O_5-WO_3/TiO_2 [13], but it suffers problems such as high manufacturing cost, heavy metal loss and secondary pollution caused by volatility at high temperature. From this, the development of low-cost and environment-friendly catalysts that replace V-Ti-based ones has attracted much attention in the energy and environment engineering field [14,15]. Till now, some progress has been made in iron-based metal oxides catalysts [16]. On the other hand, various metal oxide wastes that include red mud [17,18], fly ash [19] and aluminum dross [20] are inexpensive materials that can be directly used in catalyst preparation, among which the red mud contains abundant effective iron oxides and thereby is valuable in research on SCR deNO_x catalyst. Therefore, a systematic study is needed to assess the feasibility of red mud for SCR deNO_x in coal-fired flue gas processing.

In view of the fact that alkaline substances such as Na, K, Ca and Mg in red mud can be toxic to SCR activity caused by the poisoning of acid sites on the catalyst surface, dealkalization was applied in catalyst preparation. In addition, we noticed that cerium is an important rare earth element that can contribute to various types of catalytic reaction [21,22], and doping of Ce can increase the amount of acid sites on the catalyst surface [23,24]. Recently, Xu et al. [5] prepared cerium-modified red mud catalyst for catalytic ozonation with the result of improved activity. In our present study, Bayer red mud was used to prepare the low-cost SCR deNO_x catalyst, and on the basis of alkali-removed red mud, the denitrification characteristics of Ce-doped red mud catalysts were evaluated with simulated flue gas atmosphere. X-ray Fluorescence (XRF), X-ray Diffraction (XRD), N_2 isotherm adsorption-desorption analysis (BET), Scanning Electron Microscopy (SEM), Thermogravimetric Measurement (TG) and NH_3-Temperature Programmed Desorption (NH_3-TPD) measurements were employed to investigate the internal mechanism between the properties and performance of red mud.

2. Results

2.1. Effect of Dealkalization Method

2.1.1. Components Analysis of RM and Alkali-Removed RM

The chemical composition of red mud catalysts prepared by different dealkalization methods is shown in Table 1. In raw red mud (RM), SiO_2, Al_2O_3 and Fe_2O_3 were the major components (totaling more than 60%); the next ones were Na_2O, TiO_2, CaO and a small amount of MgO and K_2O, as well. Among them, Na and Ca oxides cause sintering in catalyst at high temperatures [7] and reduce the acidity of the catalyst surface, which is seriously toxic to the SCR catalytic activity [25]. After moderate dealkalization, red mud can be activated while most of effective substances are still preserved [26]; hence, the effect of the dealkalization method on the properties and SCR activities of red mud was studied.

Table 1. The composition of RM, WRM1, WRM2 and ARM (wt%). RM: red mud; WRM*n*: Water washing of red mud catalyst, *n* = 1, 2, refers to washing times; ARM: acid washing of red mud catalyst.

Samples	LOSS	SiO_2	Al_2O_3	Fe_2O_3	CaO	MgO	SO_3	TiO_2	K_2O	Na_2O	Others
RM	13.02	20.74	24.26	23.89	2.77	0.56	0.93	2.95	0.57	10.13	0.18
WRM1	13.75	19.75	27.81	22.61	5.52	0.37	0.85	1.55	0.07	7.43	0.29
WRM2	14.14	19.26	27.40	23.23	5.42	0.36	1.01	1.43	0.13	7.35	0.27
ARM	13.06	18.19	35.34	23.12	3.28	0.24	0.25	2.17	-	4.23	0.12

As shown in Table 1, Na and K contents in WRM1 (WRM*n*, Water washing of red mud catalyst, n = 1, 2, refers to washing times), WRM2 and ARM were found to be reduced significantly towards water washing and acid washing, but minor changes were observed between WRM1 and WRM2 towards adding washing times. It was noticed that Ca content had increased after washing as it was more insoluble in water, and its absolute quality had decreased less or even basically remained unchanged, so that the relative proportion increased. Thus, the water washing method had certain limitations, but it can be seen that the acid washing method can reduce all kinds of alkaline substances to a certain degree, which is considered acceptable for dealkalization of RM.

Figure 1 shows the XRD patterns of RM, ARM and ARM(400) (ARM(*t*), where *t* refers to the calcining temperature). The crystalline phases determined in three samples were α-Fe_2O_3 (hematite, PDF-33-0664#), TiO_2 (anatase, PDF-89-4921#), SiO_2 (quartz, PDF-46-1045#), as well as trace phases of carbonates and aluminosilicates. No obvious other diffraction peaks were found, suggesting that other components were well-dispersed in red mud. This result was in accordance with the recent research on phases of red mud produced in China [27]. In ARM, the Fe+3O(OH) (goethite, PDF-29-0713#) diffraction peaks considerably diminished, and in ARM(400), they finally vanished, which affirmed that the crystalline Fe+3O(OH) had transformed due to dehydration after the calcination process.

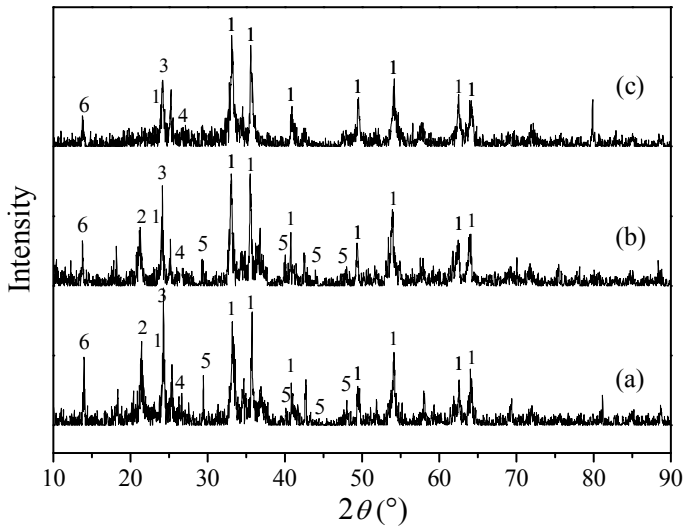

Figure 1. XRD patterns of: (**a**) RM, (**b**) ARM and (**c**) ARM(400). 1: α-Fe_2O_3; 2: Fe+3O(OH); 3: anatase (TiO_2); 4: quartz (SiO_2); 5: calcite ($CaCO_3$); 6: aluminosilicate.

2.1.2. Catalytic Activity of RM and Alkali-Removed RM

Figure 2 shows the NO_x conversion rate of RM, ARM and ARM(400) as a function of reaction temperature. In comparison with RM, the denitration efficiency of ARM increased by about 10% points in the range of 150–375 °C. Unlike the behavior of RM and ARM, better performance was acquired by ARM(400) in the range of 350–400 °C, where the active temperature window had been broadened. Thus, calcining after acid washing can reduce the adverse effect of alkali in RM and effectively improve the catalytic activity at high temperatures, which can be considered as a cost-effective treatment method.

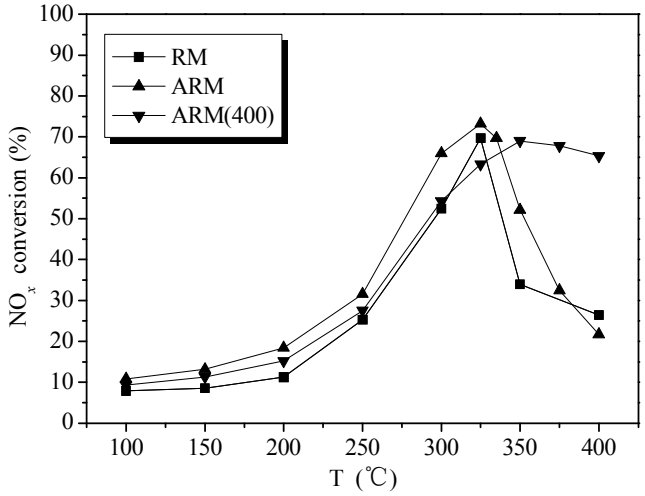

Figure 2. Catalytic activity of RM, ARM and ARM(400). Reaction conditions: reaction gas pressure = 0.1 MPa, N_2 balance, total flow = 2000 mL·min^{-1}, Gas Hourly Space Velocity (GHSV) = 30,000 h^{-1}, [NH_3/NO] = 1.0, initial concentration of NH_3, NO and O_2 = 0.05%, 0.05% and >3.5%, respectively.

2.1.3. Structure Characterization of RM and Alkali-Removed RM

Specific surface areas and pore structure are of significant importance of heterogeneous catalyst. The BET surface areas of samples are shown in Table 2. In general, dealkalization had a positive effect on the BET surface areas, but pore volumes and pore diameter decreased to a certain degree after acid washing treatment. The BET surface areas of ARM and ARM(400) were 50.54 m^2·g^{-1} and 57.19 m^2·g^{-1}, respectively. This suggests that acid washing can remove most of the alkaline substances from red mud and clear the inner channel of red mud minerals [28], so that the specific surface area can be further optimized after calcination, which is beneficial to the diffusion and adsorption of reaction gas on the catalyst surface.

Table 2. BET surface areas, pore volumes and average pore diameter of RM, ARM and ARM(400). ARM(*t*), where *t* refers to the calcining temperature.

Samples	BET Specific Surface Area (m^2·g^{-1})	Pore Volume (cm^3·g^{-1})	Average Pore Diameter (nm)
RM	42.7	0.1919	109.2
ARM	50.5	0.1048	82.9
ARM(400)	57.2	0.1041	72.8

Figure 3 shows the SEM images of samples. As shown in Figure 3a,b, WRM1 showed a similar cementation structure to RM: it displayed a large block, columnar and lamellar structure, surrounded by flocculent small particles of crystallization, where the surface of particles was rough, and the adhesion and pore structure of the catalyst had obviously collapsed and been blocked; while in Figure 3c,d, ARM had larger voids and highly-dispersed particles, owing to the displacement of impurities by H^+ occurring in mineral layers, involving K^+, Na^+, Ca^{2+} and Mg^{2+} ions. After calcination, ARM(400) had further homogeneous morphology with ball-shaped particles, and the surface became smooth and better connected, which provided a larger specific surface area and exposed sufficient active sites for gas diffusion and adsorption in the SCR reaction, and it was the significant reason for the improved activity.

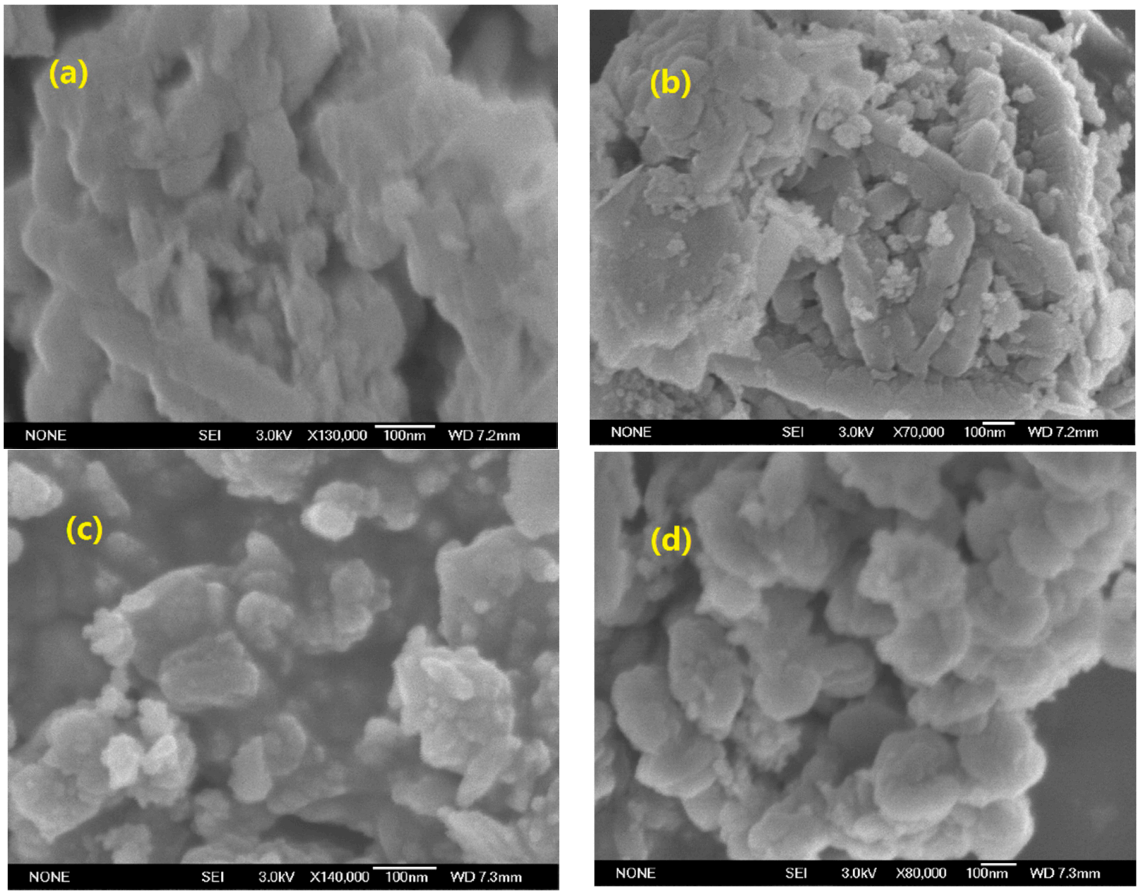

Figure 3. SEM images: (**a**) RM, (**b**) WRM1, (**c**) ARM and (**d**) ARM(400).

2.1.4. Effect of Calcination Temperature on Catalytic Activity of ARM

Calcination temperatures can affect the catalytic activity of red mud. For the TG results in Figure 4a, the fresh ARM sample had a continuous mass loss and finally stabilized at 700 °C. The weight loss peak before 100 and 200 °C corresponds to the removal of adsorbed water and crystalline water in red mud, which is necessary during calcination activation. Moreover, the weight loss stage in the range of 200–300 °C and 300–350 °C can be assigned to the removal of crystalline water from the gibbsite and goethite structure, respectively. To prevent sintering by residual alkaline substance in ARM, the calcination temperature should not exceed 600 °C, so the ARM(400), ARM(450), ARM(500) and ARM(550) catalysts were prepared to study. With the comparison of RM, their catalytic activities are illustrated in Figure 4b. The trends of the conversion-temperature curves of calcined ARM present as the same, but in the range of 200–350 °C reaction temperatures, the catalytic activity of four samples was in the order of ARM(500) > ARM(550) > ARM(400) > ARM(450). Therefore, the calcination temperature of 500 °C was chosen to prepare ARM-supported catalyst with further treatment.

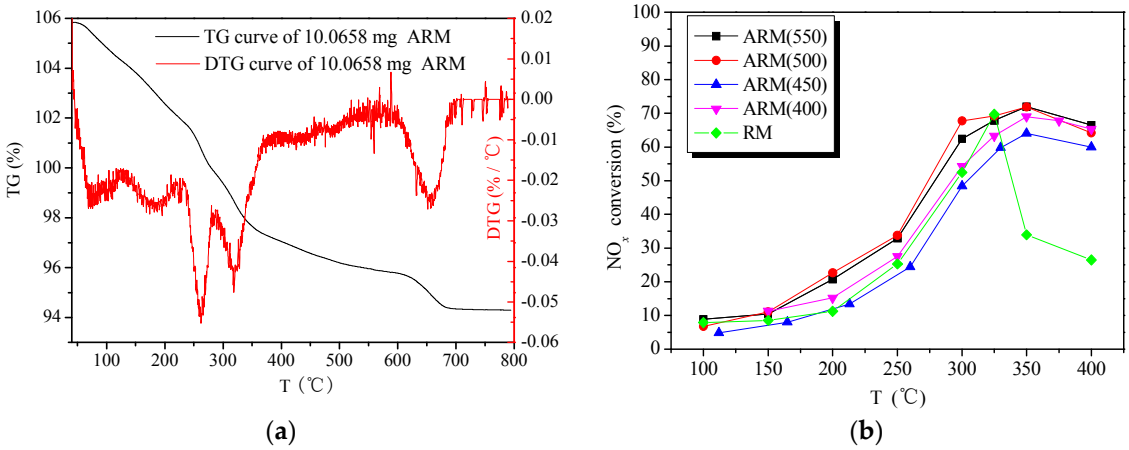

Figure 4. (**a**) The TG-DTG curves of 10.0658 mg ARM; (**b**) catalytic activity of RM, ARM(400), ARM(450), ARM(500) and ARM(550). Reaction conditions: reaction gas pressure = 0.1 MPa, N_2 balance, total flow = 2000 mL·min^{-1}, GHSV = 30,000 h^{-1}, [NH_3/NO] = 1.0, initial concentration of NH_3, NO and O_2 = 0.05%, 0.05% and >3.5%, respectively.

2.2. Effect of Ce-Doping

2.2.1. Catalytic Activity of Ce/ARM

Though ARM(500) gained a good performance in the experiments above, it still had a certain difference from commercial catalyst. In this section, Ce-doped red mud catalysts were prepared with 500 °C calcination, using ARM as a support. Figure 5 shows the catalytic activity of Ce/ARM with different Ce loading. The amount of Ce loading did not have a linear influence on activities of Ce/ARM in the whole range of reaction temperatures. Compared with ARM(500), the NO_x conversion increased by an average of 5% in $Ce_{0.1}$/ARM and by 10–20% in others. With the increase of Ce loading, the active temperature window of $Ce_{0.5}$/ARM and $Ce_{0.7}$/ARM slightly shifted to high temperatures. The highest NO_x conversion of 88% was gained by $Ce_{0.3}$/ARM at 300 °C and 90% by $Ce_{0.7}$/ARM at 350 °C. It can be viewed that red mud-based Ce/ARM catalysts have good performance for denitration in 275–400 °C, which is comparable with Ce/TiO_2 (5% Ce-doped) [29] and V_2O_5/TiO_2 catalysts [30].

Based on the above analysis, the SCR activities of Ce-doped red mud were remarkably promoted in both medium and high temperatures, and the active temperature window of catalysts had been apparently broadened. For better understanding the results of differences in activity over Ce/ARM and ARM(500), the NH_3-TPD curves are shown in Figure 6 to identify the acidity difference. Like the performance of activity presented in Figure 5, the shapes of the ARM(500) and $Ce_{0.1}$/ARM curves were similar, and a marked increase of desorption intensity was found in $Ce_{0.1}$/ARM, which definitely identified the promoting effect of Ce doping on the amount of surface acid sites and improved activity. For the peaks of the $Ce_{0.3}$/ARM sample, both the peak area of low and high temperatures dramatically increased, which was assigned to enhanced NH_3 adsorption from weak, medium and strong acid sites after further Ce doping. Combined with the analysis in Section 2.1, it is concluded that the removal of alkali and NH_3 adsorption were of great importance to the catalytic behavior of red mud owing to the changes in structure and acid sites provided by acid treatment and Ce doping, both of which favored the SCR reaction.

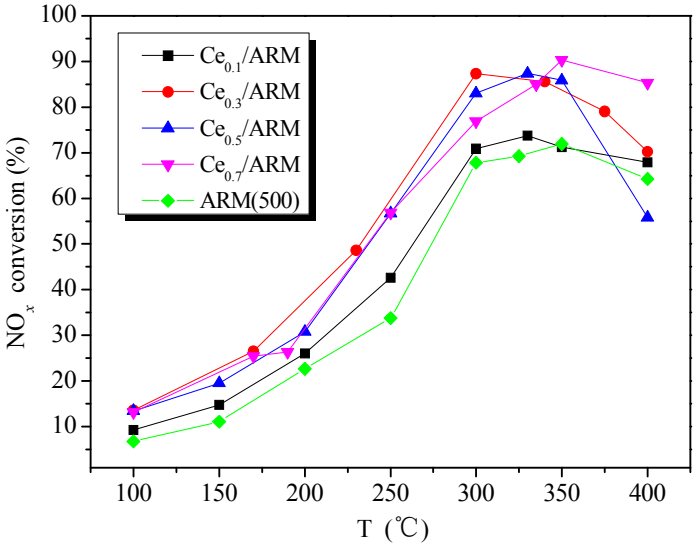

Figure 5. Catalytic activity of ARM(500) and Ce_x/ARM catalysts. Reaction conditions: reaction gas pressure = 0.1 MPa, N_2 balance, total flow = 2000 mL·min^{-1}, GHSV = 30,000 h^{-1}, [NH_3/NO] = 1.0, initial concentration of NH_3, NO and O_2 = 0.05%, 0.05% and >3.5%, respectively.

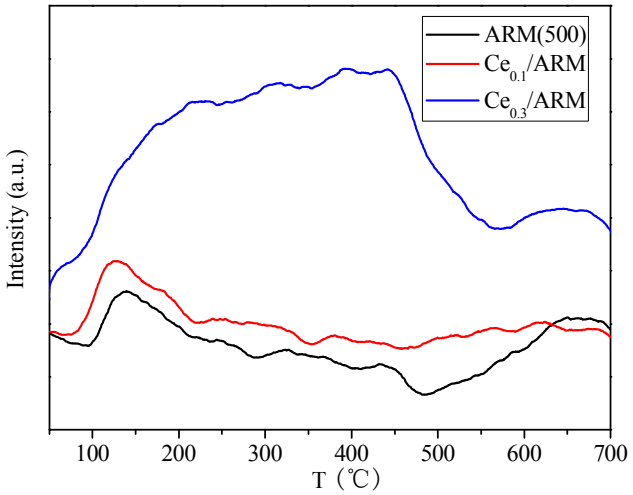

Figure 6. The NH_3-Temperature Programmed Desorption (TPD) curves of $Ce_{0.3}$/ARM, $Ce_{0.1}$/ARM and ARM(500).

2.2.2. Structure Characterization of Ce/ARM

Figure 7a shows the XRD patterns of $Ce_{0.1}$/ARM, $Ce_{0.3}$/ARM, $Ce_{0.5}$/ARM and $Ce_{0.7}$/ARM. Local patterns in the range of 40–60° are shown in Figure 7b. Compared with JCPDS standard cards, the main crystalline phase in Ce/ARM samples was α-Fe_2O_3 (PDF-33-0664#), which was consistent with the result of ARM. Moreover, diffraction peaks of CeO_2 (PDF-34-0394#) were observed, except in $Ce_{0.1}$/ARM, which had the least Ce loading. As a result, Ce species had formed the CeO_2 crystalline phase in the preparation. In all of four samples, there were no other obvious peaks, indicating that other species were well-dispersed in Ce/ARM after Ce-doping and 500 °C calcination.

According to the Scherrer Equation (1) [31], the peak width at half height (FWHM) of crystal lattice diffraction peaks is inversely proportional to the diameter of crystalline grains, so it can be deduced from the local patterns that in $Ce_{0.3}$/ARM, the average crystalline size of α-Fe_2O_3 was lower than other samples:

$$D = 0.89\lambda/(\beta\cos\theta) \quad (1)$$

where D is the average thickness of a crystalline grain perpendicular to the crystal surface; β is the FWHM of sample diffraction peaks; θ is the diffraction angle; λ is incident X-ray light wavelength of 0.154 nm.

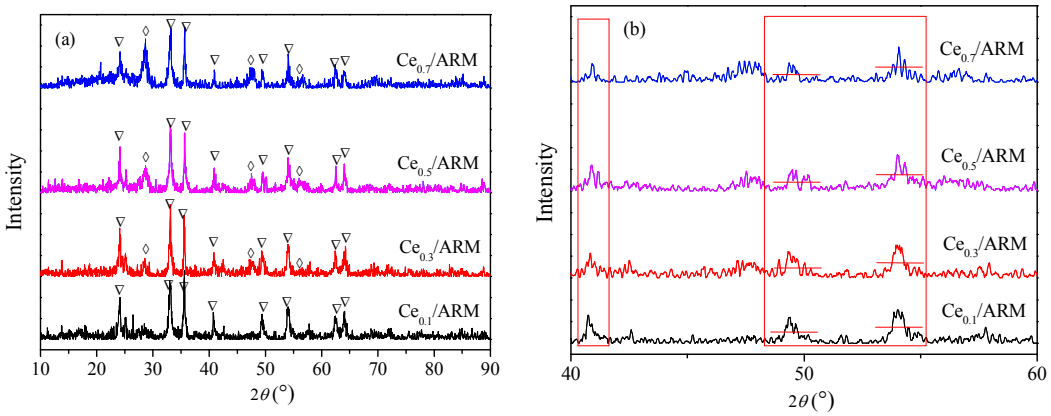

Figure 7. XRD patterns of Ce/ARM catalyst. (**a**) Complete patterns (▽: α-Fe_2O_3 ◊: CeO_2); (**b**) local patterns.

When the composition and macrostructure of catalyst are fixed, the catalytic activity is primarily affected by the specific surface area. Table 3 lists the BET surface areas of Ce/ARM.

Table 3. BET surface areas, pore volumes and average pore diameter of Ce/ARM catalysts.

Samples	BET Specific Surface Area ($m^2 \cdot g^{-1}$)	Pore Volume ($cm^3 \cdot g^{-1}$)	Average Pore Diameter (nm)
$Ce_{0.1}$/ARM	46.5	0.0922	87.9
$Ce_{0.3}$/ARM	54.4	0.1002	81.6
$Ce_{0.5}$/ARM	45.1	0.1071	98.0
$Ce_{0.7}$/ARM	46.1	0.1181	103.1

Compared to ARM (50.54 $m^2 \cdot g^{-1}$) in Table 2, The BET specific surface areas of Ce/ARM had decreased to some degree, yet it was calculated that the crystalline grain diameter of α-Fe_2O_3 of Ce/ARM dropped to 15–30 nm compared to that of ARM. In the case of this study, $Ce_{0.3}$/ARM not only had low crystalline grain diameter, but also provided larger BET specific surface area (54.4 $m^2 \cdot g^{-1}$), as well as enhanced the surface acidity, which consequently improved the catalytic activity just under a simple preparation method with a small amount of Ce-doping (less than 5%).

2.2.3. NH_3 and O_2 Transient Response of $Ce_{0.3}$/ARM and the Effect of Major Operating Parameters

As shown in Figure 8a–e, the fresh $Ce_{0.3}$/ARM catalyst was selected to investigate the effect of major operating parameters on its performance. The experiments were conducted at a reaction temperature of 300 °C, where they could gain the highest denitration efficiency.

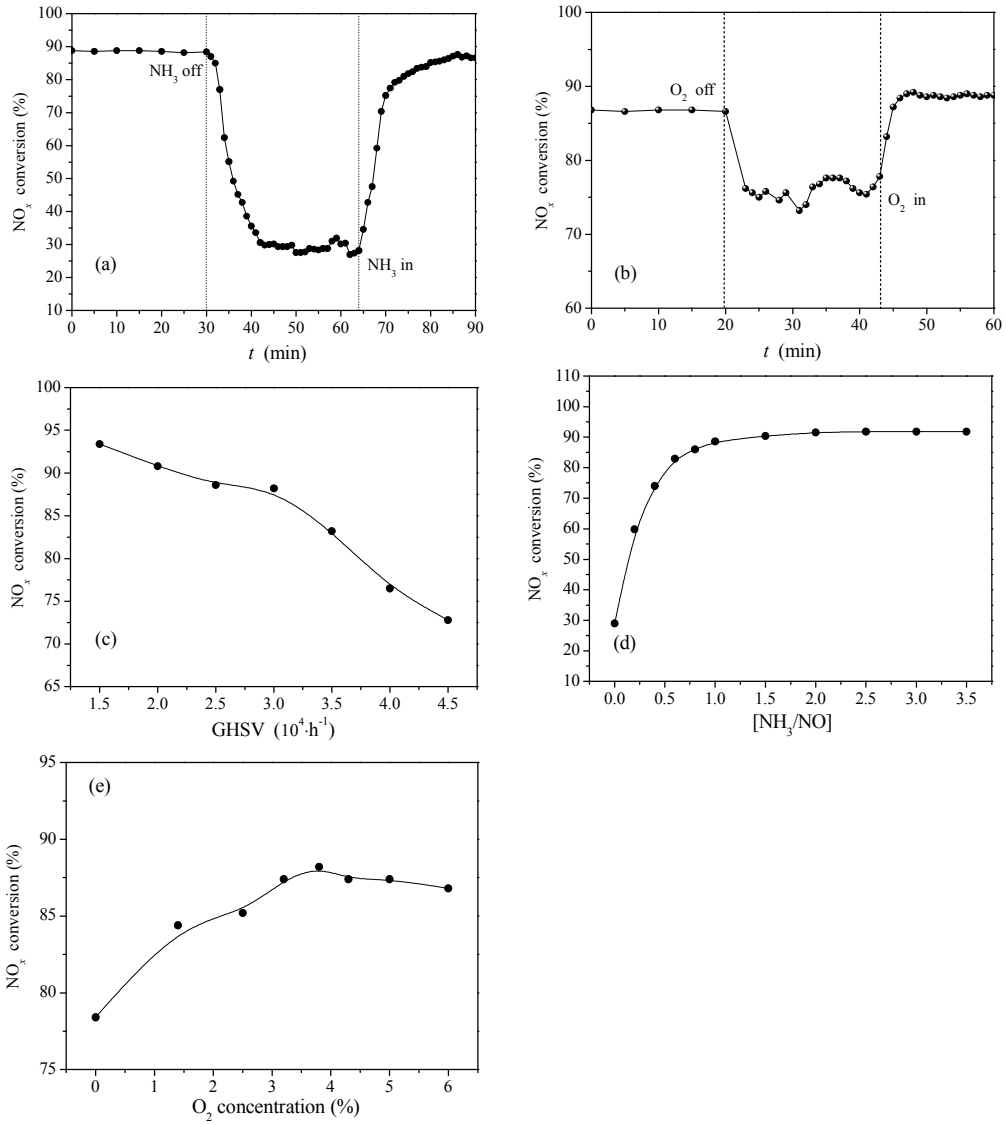

Figure 8. $Ce_{0.3}$/ARM catalyst: (**a**) NH_3 transient response; (**b**) O_2 transient response. Reaction conditions: reaction temperature = 300 °C, reaction gas pressure = 0.1 MPa, N_2 balance, total flow = 2000 mL·min^{-1}, GHSV = 30,000 h^{-1}, [NH_3/NO] = 1.0, initial concentration of NH_3, NO and O_2 = 0.05%, 0.05% and >3.5%, respectively. (**c**) Effect of GHSV. Reaction conditions: reaction temperature = 300 °C, reaction gas pressure = 0.1 MPa, N_2 balance, total flow = 2000 mL·min^{-1}, GHSV = 15,000–30,000 h^{-1}, [NH_3/NO] = 1.0, initial concentration of NH_3, NO and O_2 = 0.05%, 0.05% and >3.5%, respectively. (**d**) Effect of [NH_3/NO]. Reaction conditions: reaction temperature = 300 °C, reaction gas pressure = 0.1 MPa, N_2 balance, total flow = 2000 mL·min^{-1}, GHSV = 30,000 h^{-1}, [NH_3/NO] = 0–3.5, initial concentration of NH_3, NO and O_2 = 0.05%, 0.05% and >3.5%, respectively. (**e**) Effect of O_2 volume fraction. Reaction conditions: reaction temperature = 300 °C, reaction gas pressure = 0.1 MPa, N_2 balance, total flow = 2000 mL·min^{-1}, GHSV = 30,000 h^{-1}, [NH_3/NO] = 0–3.5, initial concentration of NH_3, NO and O_2 = 0.05%, 0.05% and 0–6%, respectively.

As is known from the NH_3-SCR reaction Equations (2)–(5), insufficient NH_3 will lead to inadequate SCR reaction and low NO_x conversion. Figure 8a shows the transient response of NH_3 on $Ce_{0.3}$/ARM. In the initial half-hour experiment, the whole of the reaction gas was thoroughly mixed and flowed through the catalyst bed for a steady-state reaction. When the NH_3 feed was instantly cut off at 30 min, there was hardly a concentration of gaseous NH_3 in the flow, but NO_x conversion did not drop immediately till it declined to lower than 30% 12 min later, which was attributed to residual

adsorbed NH_3 continuously reacted with NO; it also demonstrated that in this period, the adsorbed NH_3 was quickly consumed in the complete SCR reaction. After the plateau between 42 min and 62 min, the NH_3 feed was turned on. NO_x conversion rapidly raised at the beginning of 5 min, then slowly increased and finally recovered after 20 min. Overall, the adsorption of NH_3 on the catalyst surface played an important role in the SCR reaction on $Ce_{0.3}$/ARM catalyst, which clearly agreed with the requirement of acid sites for improved SCR activity, as discussed above in Figure 6.

$$4NH_3 + 4NO + O_2 \rightarrow 4N_2 + 6H_2O \quad (2)$$

$$4NH_3 + 2NO_2 + O_2 \rightarrow 3N_2 + 6H_2O \quad (3)$$

$$4NH_3 + 6NO \rightarrow 5N_2 + 6H_2O \quad (4)$$

$$8NH_3 + 6NO_2 \rightarrow 7N_2 + 12H_2O \quad (5)$$

According to "standard SCR" and "fast SCR" Equations (2) and (3) [32], the SCR reaction occurs more quickly in the presence of O_2. As seen from Figure 8b, NO_x conversion dropped and recovered immediately when the O_2 feed was instantly cut off and turned on, which indicated that gaseous O_2 reacted on the catalyst surface. During the time interval between 22 min and 43 min, the NO_x conversion of $Ce_{0.3}$/ARM remained as high as 78%, which may result from the superior capacity for cyclic oxygen storage and redox of CeO_2 formed in red mud, which ensured that there were sufficient adsorbed oxygen and lattice oxygen participating in the SCR reaction and contributing to the performance of $Ce_{0.3}$/ARM.

Figure 8c shows the effect of Gas Hourly Space Velocity (GHSV) on the catalytic activity of $Ce_{0.3}$/ARM. Different GHSV was generated by changing the filling volume of catalysts. Before GHSV of 30,000 h^{-1}, NO_x conversion remained more than 88% and decreased slightly with the increase of flue gas flow velocity, but it obviously dropped in GHSV of 30,000–45,000 h^{-1}, because when using a small amount of catalyst, the residence time was too short to make the reaction gas fully contact the catalyst surface. The results showed that the $Ce_{0.3}$/ARM catalyst was adapted to GHSV of 15,000–30,000 h^{-1}.

Figure 8d shows the effect of [NH_3/NO]. In the presence of NH_3, the NO_x conversion increased sharply and reached 74% with [NH_3/NO] of 1:2 (0.5), and it reached nearly 90% with [NH_3/NO] of 1.0, then stayed at the same level with the increase of [NH_3/NO] before 3.5%. To save the NH_3 consumption and considering the efficiency, it is best to control the [NH_3/NO] at 1.0, which also reveals that the reaction on the catalyst surface of $Ce_{0.3}$/ARM followed the stoichiometric ratio of the "standard SCR" reaction.

Figure 8e shows the effect of O_2 concentration. In accordance with the result in Figure 7b, the NO_x conversion of $Ce_{0.3}$/ARM maintained about 75% in absence of O_2, and it further raised as the O_2 concentration increased. According to "fast SCR" Equation (3), with excessive O_2, NO could be oxidized to NO_2, which accelerates the SCR reaction rate and enhances the NO_x conversion. In this work, the initial O_2 concentration of 3.5–4% in atmosphere is appropriate, where the NO_x conversion of $Ce_{0.3}$/ARM was the best.

2.2.4. Effect of SO_2 on Catalytic Activity of $Ce_{0.3}$/ARM

As shown in Figure 9, a twelve-hour stability experiment of SO_2 resistance was carried out at 300 °C to primarily investigate the effect of SO_2 on the catalytic behaviors of $Ce_{0.3}$/ARM, and another experiment of fresh catalyst without SO_2 was done as a comparison. Starting with 0.03% SO_2, the NO_x conversion decreased obviously from 90–85% in 30 min, then gradually dropped to 73% in the following 2.5 h and maintained a plateau. The inhibition on activity during those 6 h could be explained by competitive adsorption of SO_2 on reaction active sites and continued blocking of the intermediate product. After SO_2 was cut off, the NO_x conversion did not recover and finally stabilized at 64%, which indicated that SO_2 had led to irreversible sulfate deposition or metal sulfate species

formation [33] on $Ce_{0.3}$/ARM, so that some active sites were blocked. Thus, the SO_2 resistance features of $Ce_{0.3}$/ARM need further development in the future.

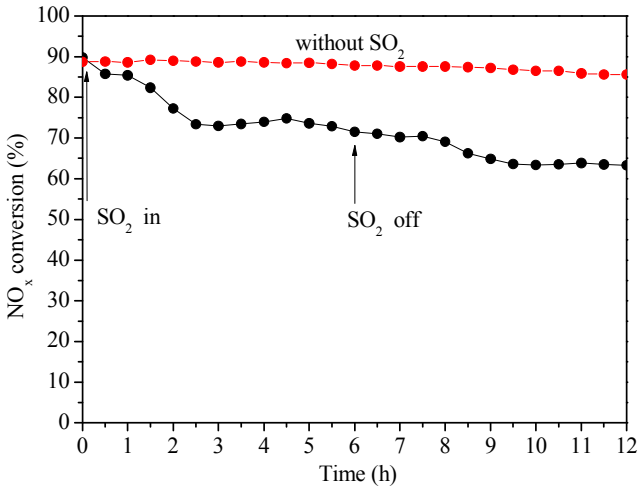

Figure 9. Catalytic activity of $Ce_{0.3}$/ARM in the presence of SO_2 and without SO_2. Reaction conditions: Reaction temperature = 300 °C, reaction gas pressure = 0.1 MPa, N_2 balance, total flow = 2000 mL·min^{-1}, GHSV = 30,000 h^{-1}, [NH_3/NO] = 1.0, initial concentration of NH_3, NO, O_2 and SO_2 = 0.05%, 0.05%, >3.5% and 0.03%, respectively.

3. Discussion

Admittedly, the results in this work demonstrated the advantages of $Ce_{0.3}$/ARM catalyst for simple preparation and promising application in medium and high temperature denitration with typical compositions of flue gas, but the problem of inferior SO_2 resistance should be overcome for the purpose of practical use; further study is still needed on its performance in actual flue gas, where the effects of H_2O and fly ash cannot be ignored. Moreover, the polymetallic property of red mud will increase its uncertainty of activity, which remains to be investigated. In the case of this study, it can be concluded that treated red mud was a feasible support for Ce-doped NH_3-SCR catalyst, and the effects of the dealkalization method and Ce doping on structure and surface acidity had been discussed. In a next step, a point-by-point comparison with previous work should be made.

Recently, in an important progress [8] related to red mud-based (also received from the Shandong Aluminum Industry) SCR catalyst, a variety of samples prepared were investigated, which showed some controversial results at first glance. However, the distinction of work between those samples and this study should be considered in detail, which is shown in Table 4.

Table 4. Comparison of works.

Options	Reference [8]	This Study
Synthesis method	acid-base neutralization	acid washing; impregnation
Activation treatment	washing, drying and calcination; SO_2-activated	washing, drying and calcination
Catalyst composition	Fe_2O_3-TiO_2/(SiO_2-Al_2O_3) (RM-based catalyst)	Ce-doped mixed oxides with inevitable residual alkali (Ce/ARM)
Major active component	α-Fe_2O_3, $Fe_2(SO_4)_3$	α-Fe_2O_3, CeO_2 and others
Active temperature window	350–450 °C	275–375 °C
Operating conditions	GHSV of 60,000 h^{-1}	GHSV of 30,000 h^{-1}

On account of different catalyst precursors, this may explain the reason why the activity of the RM-based catalyst increased with a lower calcination temperature in the range of 500–600 °C [8], but a relatively high temperature was chose from 400–600 °C for ARM, because a relatively lower calcination temperature may be needed for suitably phase structure transformation of the metal hydroxide formed by the neutralization method, while for impregnated catalyst, a low calcination temperature will make it inadequate to establish a strong interaction between the active component and catalyst support. In addition, conflicting performance is also observed between the SO_2 resistance of SO_2–activated RM and $Ce_{0.3}$/ARM. For one thing, increasing the GHSV could indeed reduce the risk of ammonium sulfate deposition. For another, the inferior performance of $Ce_{0.3}$/ARM, by contrast, is possibly due to the fact that some ammonium sulfate could not completely decompose at 300 °C, where the stability experiment was carried out, but the $Ce_{0.3}$/ARM catalyst had the best efficiency at that temperature, so adding a low-temperature sulfur-resistant component to existing $Ce_{0.3}$/ARM catalyst or improving its high-temperature activities will have a good prospect in future work. Nevertheless, SO_2 activation may also have a promoting effect on $Ce_{0.3}$/ARM, though at present, it still lacks the understanding of the interaction between SO_2 and the mixture of metal oxides in red mud.

Furthermore, better understanding of the effect of alkaline substances in red mud on SCR behaviors should be made to help confirm the real reaction sites and even tune the catalyst properties. An interesting work [34] proposed the idea that the surface basicity of K-deposited Ce-supported sulfated zirconia catalyst could also promote the NO conversion especially in a relatively lower temperature range by enhancing the adsorption and oxidation of NO as long as sufficient surface acidity was available, which gives inspiration to improve the activity of existing Ce/ARM catalyst. Herein, the assisted component in red mud could be designed with respect to a certain study object in future work.

4. Materials and Methods

4.1. Preparation of RM and Alkali-Removed RM

Raw red mud catalyst (RM): Bayer red mud was received from Shandong Aluminum Industry Corporation (Zibo, China). The uniform powdered red mud was obtained by crushing and grinding received red mud, then it was screened by 50–120 mesh, after which a small amount of deionized water was added to make powders into strip granules, followed by air drying at 105 °C for 6 h. Finally, the catalyst particles of RM were obtained via screening by 40–60 mesh (0.25–0.38 mm) [35] from those broken strips.

Water washing of red mud catalyst (WRM*n*, *n* = 1, 2, refers to washing times): The above-mentioned powdered red mud and deionized water were stirred in a liquid-solid ratio of 10 $mL \cdot g^{-1}$ to form a slurry, with heating in an 80 °C water bath. The resulting solution was washed *n* times with deionized water by the vacuum filtration method until the pH of filtrate reached 7.0, and then, the filter cake was air dried at 105 °C for 6 h until the weight was constant. Finally, the catalyst particles of WRM*n* were obtained via grinding and screening by 40–60 mesh from the dried cake.

Acid washing of red mud catalyst (ARM): The prepared red mud slurry was washed once and then titrated with 0.2 mol/L HNO_3 until the pH of the solution reached 7.0. The resulting solution was repeatedly washed to remove residual ions and impurities until the pH of the filtrate reached 7.0, and then, the filter cake was air dried at 105 °C for 6 h until the weight was constant. Finally, the catalyst particles of ARM were obtained via grinding and screening by 40–60 mesh from the dried cake.

In addition, some of the ARM catalyst particles were treated by calcining in air at different temperatures (400 °C, 450 °C, 500 °C and 550 °C) for 4 h. The obtained catalysts were defined as ARM(*t*), where *t* refers to the calcining temperature.

4.2. Preparation of Ce-Doped Red Mud Catalyst

Ce-doped red mud catalysts (Ce_x/ARM, x refers to the impregnated solution concentration, for which the unit is mol·L^{-1}) were prepared by the impregnation method, using a certain amount of $Ce(NO_3)_3$ solution mixed with ARM powders in a liquid-solid ratio of 1 mL·g^{-1}, followed by stirring for 1 h and ultrasonic treatment for 30 min. The resulting slurry was dried rapidly for 20 min by microwaving with a power of 210 W and then air dried at 105 °C for 6 h until the weight was constant. After that, the dried bulk was treated by calcining in air at 500 °C for 4 h. Finally, the Ce/ARM catalyst particles were obtained via grinding and screening by 40–60 mesh from the bulk. Table 5 lists the actual weight percentage of Ce content in red mud catalysts.

Table 5. Ce content in Ce/ARM catalysts.

Samples	Ce Content (wt%)
$Ce_{0.1}$/ARM	1.40
$Ce_{0.3}$/ARM	4.20
$Ce_{0.5}$/ARM	7.01
$Ce_{0.7}$/ARM	9.81

4.3. Catalytic deNO$_x$ Activity Measurements

The NH_3-SCR denitration reaction was carried out on a fixed-bed flow reactor that contained a vertical quartz tube, 0.8 cm inside diameter and 60 cm in length, fitted within a temperature-controlling (room temperature to 400 °C available) electrical heating furnace. Four milliliters of the catalyst sample particles were loaded on a quartz baffle plate fixed on the constant temperature area of the tube, and a K-type thermocouple was inserted in the catalyst bed to measure the accurate catalyst temperature. Simulated coal-fired SCR flue gas consisted of NH_3, NO and O_2, in volume fractions of 0.05% (500 ppm), 0.05% and more than 3.5%, respectively. Industrial nitrogen was used as the carrier gas. Total flow into the reactor was controlled as 2000 mL·min^{-1}, and the Gas Hourly Space Velocity (GHSV) was 30,000 h^{-1}. Before each experiment point at different reaction temperature (T, °C), reaction gas was thoroughly mixed and flowed through the catalyst bed for 30 min to avoid the measurement error of concentration caused by gas adsorption. Catalytic deNO$_x$ activity of red mud was evaluated by the NO$_x$ conversion rate:

$$\mathrm{NO}_x\ \mathrm{Conversion}(\%) = [(NO_x(inlet) - NO_x(outlet))/NO_x(inlet)] \times 100\% \quad (6)$$

where $NO_x(inlet)$ and $NO_x(outlet)$ signifies the inflow and outflow NO$_x$ (NO and NO_2) concentrations which were measured by the MGA Flue Gas Analyzer (MRU Corporation, Neckarsulm, Obereisesheim, Germany).

4.4. Characterization of Catalysts

The component of samples was analyzed by X-ray Fluorescence (XRF) using the ZSX Primus II Analyzer (Rigaku Corporation, Tokyo, Japan). The crystal structure of samples was examined by X-ray Diffraction (XRD) using the D/max 2500 PC Diffractometer (Rigaku Corporation, Tokyo, Japan) equipped with Cu $K\alpha$ radiation with a wavelength of 0.154 nm. The samples were investigated in the 2θ range of 10–90° at a scanning speed of 1.2°·min^{-1}, using the MDI Jade software to analyze phases. The Brunauer–Emmett–Teller (BET) specific surface area and pore volume of samples were determined by N_2 isotherm adsorption-desorption using the ASAP2020 Surface Area and Porosity Analyzer (Micromeritics Corporation, Norcross, GA, USA). The microscopic morphology of samples was observed by scanning electron microscope (SEM) using the SUPRA 55 Instrument (ZEISS, Oberkochen, Germany). The calcining parameters were decided by Thermogravimetric Measurement (TG) using

the TGA/SDTA851 Analyzer (Mettler Toledo, Zurich, Switzerland) under nitrogen atmosphere and a heating rate of 15 °C·min^{-1} from room temperature to 800 °C.

The NH_3-TPD experiments were performed on a ChemAuto 2920 Instrument (Micromeritics, Norcross, GA, USA). First, 90 mg of sample were loaded on a quartz U-tube and heated from room temperature to 300 °C for an hour in argon atmosphere, then cooled to 50 °C. After blowing of argon for 30 min, 10 vol% NH_3 (Ar balance) was switched on to complete the pre-absorption for 30 min and heated to 100 °C for 60 min with argon blowing. After the baseline was smooth, the NH_3-TPD test was performed by heating the sample to 700 °C at 5 °C·min^{-1}. The desorption amount was detected by the TCD detector. When the test finished, the argon atmosphere was switched on for natural cooling.

5. Conclusions

In this study, Bayer red mud from industrial waste was prepared as low-cost red mud-based catalyst to evaluate the performance of denitration with simulated coal-fired flue gas. It was proven that red mud was a feasible material for the NH_3-SCR catalyst.

Compared with RM and alkali-removed RM, acid washing and calcining comprised a cost-effective treatment process for raw red mud, which reduced the alkali content and improved the catalytic activity of ARM at high temperatures. The increase of BET surface area was attributed to the unobstructed catalyst pore and the homogeneous particle morphology with dispersion.

In Ce/ARM, doping of Ce significantly enhanced NH_3 adsorption from weak, medium and strong acid sites, reduced the crystallinity of α-Fe_2O_3 in ARM, optimized the specific surface area and broadened the active temperature window. The optimum doping amount was acquired by $Ce_{0.3}$/ARM, in which the NO_x conversion rate increased by an average of nearly 20% points between 250 and 350 °C, and the highest denitration efficiency reached 88% at 300 °C. The optimum conditions for the denitration reaction on $Ce_{0.3}$/ARM catalyst were controlled as follows: GHSV of 30,000 h^{-1}, O_2 volume fraction of 3.5–4% and [NH_3/NO] of 1.0.

Acknowledgments: This research was supported by the National Natural Science Foundation of China (NSFC: 51576117) and the Interdisciplinary Development Program of Shandong University (2015JC024).

Author Contributions: Jingkun Wu conceived of and designed the experiments. Jingkun Wu performed the experiments. Zhiqiang Gong, Chunmei Lu and Shengli Niu gave technical support and conceptual advice. Jingkun Wu wrote the paper. Jingkun Wu, Chunmei Lu and Zhiqiang Gong revised the paper. Kai Ding, Liting Xu and Kang Zhang contributed reagents/materials/analysis tools.

Conflicts of Interest: The authors declare no conflict of interest.

References

1. Hu, Z.P.; Zhao, H.; Gao, Z.M.; Yuan, Z.Y. High-surface-area activated red mud supported Co_3O_4 catalysts for efficient catalytic oxidation of CO. *RSC Adv.* **2016**, *6*, 94748–94755. [CrossRef]
2. Hu, Z.P.; Zhu, Y.P.; Gao, Z.M.; Wang, G.X.; Liu, Y.P.; Liu, X.Y.; Yuan, Z.Y. CuO catalysts supported on activated red mud for efficient catalytic carbon monoxide oxidation. *Chem. Eng. J.* **2016**, *302*, 23–32. [CrossRef]
3. Paredes, J.R.; Ordonez, S.; Vega, A.; Diez, F.V. Catalytic combustion of methane over red mud-based catalysts. *Appl. Catal. B* **2004**, *47*, 37–45. [CrossRef]
4. Bento, N.I.; Santos, P.S.C.; de Souza, T.E.; Oliveira, L.C.A.; Castro, C.S. Composites based on PET and red mud residues as catalyst for organic removal from water. *J. Harzard. Mater.* **2016**, *314*, 304–311. [CrossRef] [PubMed]
5. Xu, B.B.; Qi, F.; Sun, D.Z.; Chen, Z.L.; Robert, D. Cerium doped red mud catalytic ozonation for bezafibrate degradation in wastewater: Efficiency, intermediates, and toxicity. *Chemosphere* **2016**, *146*, 22–31. [CrossRef] [PubMed]
6. Koumanova, B.; Drame, M.; Popangelova, M. Phosphate removal from aqueous solutions using red mud wasted in bauxite Bayer's process. *Resour. Conserv. Recycl.* **1997**, *19*, 11–20. [CrossRef]
7. Ordonez, S.; Sastre, H.; Diez, F.V. Characterisation and deactivation studies of sulfided red mud used as catalyst for the hydrodechlorination of tetrachloroethylene. *Appl. Catal. B* **2001**, *29*, 263–273. [CrossRef]

8. Li, C.M.; Zeng, H.; Liu, P.L.; Yu, J.; Guo, F.; Xu, G.W.; Zhang, Z.G. The recycle of red mud as excellent SCR catalyst for removal of NO_x. *RSC Adv.* **2017**, *7*, 53622–53630. [CrossRef]
9. Cao, J.L.; Wang, Y.; Li, G.J.; Li, K.; Wang, Y.; Ma, M. Mesoporous modified red mud supported CuO nanocatalysts for carbon monoxide oxidation. *Curr. Nanosci.* **2015**, *11*, 413–418. [CrossRef]
10. Lamonier, J.F.; Leclerco, G.; Dufour, M.; Leclercq, L. Utilization of red mud. Catalytic properties in selective reduction of nitric oxide by ammonia. Récents Progrès en Génie des Procédés, Boues industrielles: Traitements. *Recents Prog. Genie Procedes* **1995**, *43*, 31–36.
11. Bhattacharyya, A.; Rajanikanth, B.S. Discharge plasma combined with bauxite residue for biodiesel exhaust cleaning: A case study on NO_x removal. *IEEE Trans. Plasma Sci.* **2015**, *43*, 1974–1982. [CrossRef]
12. Bhattacharyya, A.; Rajanikanth, B.S. Biodiesel exhaust treatment with HFAC plasma supported by red mud: Study on DeNO_x and power consumption. *Energy Procedia* **2015**, *75*, 2371–2378. [CrossRef]
13. Liu, X.; Li, J.H.; Li, X.; Peng, Y.; Wang, H.; Jiang, X.M.; Wang, L.W. NH_3 selective catalytic reduction of NO: A large surface TiO_2 support and its promotion of V_2O_5 dispersion on the prepared catalyst. *Chin. J. Catal.* **2016**, *37*, 878–887. [CrossRef]
14. Li, J.H.; Chang, H.Z.; Ma, L.; Hao, J.M.; Yang, R.T. Low-temperature selective catalytic reduction of NO_x with NH_3 over metal oxide and zeolite catalysts—A review. *Catal. Today* **2011**, *175*, 147–156. [CrossRef]
15. Liu, C.; Shi, J.W.; Gao, C.; Niu, C.M. Manganese oxide-based catalysts for low-temperature selective catalytic reduction of NO_x with NH_3: A review. *Appl. Catal. A* **2016**, *522*, 54–69. [CrossRef]
16. Liang, H.; Gui, K.T.; Zha, X.B. DRIFTS study of γ-Fe_2O_3 nano-catalyst for low-temperature selective catalytic reduction of NO_x with NH_3. *Can. J. Chem. Eng.* **2016**, *94*, 1668–1675. [CrossRef]
17. Sushil, S.; Batra, V.S. Modification of red mud by acid treatment and its application for CO removal. *J. Harzard. Mater.* **2012**, *203–204*, 264–273. [CrossRef] [PubMed]
18. Wang, S.B.; Ang, H.M.; Tade, M.O. Novel applications of red mud as coagulant, adsorbent and catalyst for environmentally benign processes. *Chemosphere* **2008**, *72*, 1621–1635. [CrossRef] [PubMed]
19. Xuan, X.P.; Yue, C.T.; Li, S.Y.; Yao, Q. Selective catalytic reduction of NO by ammonia with fly ash catalyst. *Fuel* **2003**, *82*, 575–579. [CrossRef]
20. Das, B.R.; Dash, B.; Tripathy, B.C.; Bhattacharya, I.N.; Das, S.C. Production of η-alumina from waste aluminium dross. *Miner. Eng.* **2007**, *20*, 252–258. [CrossRef]
21. Zhao, H.; Zhang, D.X.; Wang, F.F.; Wu, T.T.; Gao, J.S. Modification of ferrite-manganese oxide sorbent by doping with cerium oxide. *Process Saf. Environ.* **2008**, *86*, 448–454. [CrossRef]
22. Gao, X.; Jiang, Y.; Zhong, Y.; Luo, Z.Y.; Cen, K.F. The activity and characterization of CeO_2-TiO_2 catalysts prepared by the sol-gel method for selective catalytic reduction of NO with NH_3. *J. Harzard. Mater.* **2010**, *174*, 734–739. [CrossRef] [PubMed]
23. Liu, X.; Li, J.H.; Li, X.; Peng, Y.; Wang, H.; Jiang, X.M.; Wang, L.W. Mechanism of selective catalytic reduction of NO_x with NH_3 over CeO_2-WO_3 catalysts. *Chin. J. Catal.* **2011**, *32*, 836–841.
24. Wang, X.B.; Zhang, L.; Wu, S.G.; Zou, W.X.; Yu, S.H.; Shao, Y.; Dong, L. Promotional effect of Ce on iron-based catalysts for selective catalytic reduction of NO with NH_3. *Catalysts* **2016**, *6*, 112. [CrossRef]
25. Xu, C.H.F.; Chen, K.H.; Gu, Z.F.; Ma, D.D.; Rao, G.H. Effect of operation conditions on activity of de-NO_x SCR catalysts before and after poisoned by alkali metal. *Adv. Mater. Res.* **2014**, *955–959*, 702–705.
26. Seo, P.W.; Cho, S.P.; Hong, S.H.; Hong, S.C. The influence of lattice oxygen in titania on selective catalytic reduction in the low temperature region. *Appl. Catal. A* **2010**, *380*, 21–27. [CrossRef]
27. Cao, S.T.; Ma, H.J.; Zhang, Y.; Chen, X.F.; Zhang, Y.F.; Zhang, Y. The phase transition in bayer red mud from China in high caustic sodium aluminate solutions. *Hydrometallurgy* **2013**, *140*, 111–119. [CrossRef]
28. Cengeloglu, Y.; Tor, A.; Ersoz, M.; Arslan, G. Removal of nitrate from aqueous solution by using red mud. *Sep. Purif. Technol.* **2006**, *51*, 374–378. [CrossRef]
29. Xu, W.Q.; Yu, Y.B.; Zhang, C.B.; He, H. Selective catalytic reduction of NO by NH_3 over a Ce/TiO_2 catalyst. *Catal. Commun.* **2008**, *9*, 1453–1457. [CrossRef]
30. Georgiadou, I.; Papadopoulou, C.; Matralis, H.K.; Voyiatzis, G.A.; Lycourghiotis, A.; Kordulis, C. Preparation, characterization, and catalytic properties for the SCR of NO by NH_3 of V_2O_5/TiO_2 catalysts prepared by equilibrium deposition filtration. *J. Phys. Chem. B* **1998**, *102*, 8459–8468. [CrossRef]
31. Mamulova, K.K.; Tokarsky, J.; Kovar, P.; Vojteskova, S.; Kovarova, A.; Smetana, B.; Kukutschova, J.; Capkova, P.; Matejka, V. Preparation and characterization of photoactive composite kaolinite/TiO_2. *J. Harzard. Mater.* **2011**, *188*, 212–220. [CrossRef] [PubMed]

32. Iwasaki, M.; Shinjoh, H. A comparative study of "standard", "fast" and "NO_2" SCR reactions over Fe/zeolite catalyst. *Appl. Catal. A* **2010**, *390*, 71–77. [CrossRef]
33. Jiang, B.Q.; Wu, Z.B.; Liu, Y.; Lee, S.C.; Ho, W.K. DRIFT study of the SO_2 effect on low-temperature SCR reaction over Fe-Mn/TiO_2. *J. Phys. Chem. C* **2010**, *114*, 4961–4965. [CrossRef]
34. Wang, H.Q.; Gao, S.; Yu, F.X.; Liu, Y.; Weng, X.L.; Wu, Z.B. An effective way to control the performance of a ceria-based deNO_x catalyst with improved alkali resistance: Acid-base adjusting. *J. Phys. Chem. C* **2015**, *119*, 15077–15084. [CrossRef]
35. Xiong, Z.B.; Lu, C.M.; Guo, D.X.; Zhang, X.L.; Han, K.H. Selective catalytic reduction of NO_x with NH_3 over iron-cerium mixed oxide catalyst: Catalytic performance and characterization. *J. Chem. Technol. Biotechnol.* **2013**, *88*, 1258–1265.